Tandem Electrocatalytic CO_2 Reduction inside a Membrane with Enhanced Selectivity for Ethylene

Tania Akter, Hanqing Pan, and Christopher J. Barile*

Department of Chemistry, University of Nevada, Reno, NV 89557

*E-mail: cbarile@unr.edu

Abstract

In this study, electrochemical reduction of carbon dioxide (CO_2) is carried out on tandem electrodes consisting of Ag, Cu-based nanoparticles, and a proton-permeable membrane to selectively produce ethylene (C_2H_4) with Faradaic efficiencies up to 80%. We demonstrate that the origin of this high selectivity arises from the tandem architecture utilized. In particular, CO_2 is first reduced to CO on Ag, and the CO is subsequently reduced to C_2H_4 on the surface of the Cu-based nanoparticles. CO_2 reduction products were quantified, and experiments were carried out as a function of voltage, the membrane overlayer thickness, and the oxidation state of Cu in the nanoparticles. Together these results lay a framework for the selective production of value-added products from CO_2 reduction using membrane-modified tandem electrocatalysis.

Keywords: CO_2 reduction, electrocatalysis, tandem catalysis, ethylene, Nafion

Introduction

The electrochemical transformation of carbon dioxide (CO_2) into carbon-based fuels is a viable pathway to generate value-added products using renewably sourced electricity. The production of multi-carbon and oxygenated compounds from the reduction of CO_2 has the benefit of mitigating deleterious greenhouse gas emissions and lessening our reliance on fossil fuels.[1] In this manner, the electrochemical reduction of CO_2 to hydrocarbons or other fuels via multiple electron transfer mechanisms is a promising approach to develop a global carbon emission recycling scheme.[2]

Cu-based materials are the current state-of-the-art catalysts capable of reducing CO_2 to multi-carbon products. Since Hori's pioneering work on electrochemical reduction of CO_2 on metal electrodes in the 1980's, Cu-based catalysts are the main family of materials capable of producing C2+ compounds as major products.[3-11] However, Cu catalysts still suffer from low Faradaic efficiency and production rates of C2+ products. Some methods to improve CO_2 reduction selectivity using Cu electrodes are to use bimetallic electrodes, surface modification, doping, ligand substitution, and crystal structure engineering.[12, 13]

The production of C2+ and oxygenated compounds is preferred over C1 products because they have higher energy density. For example, ethylene (C_2H_4) is an important chemical feedstock for preparing plastics, ethylene oxide, and diesel fuels.[14] To improve the yield and selectivity of C_2H_4 from CO_2 electroreduction, Cu catalysts can be doped with Sn.[14] Alternatively, the crystal phase,[15-18] shape,[19] or oxidation state of Cu can be tuned to increase C_2H_4 yield.[20, 21] Polymers and organic compounds such as polyamines or triazoles can be incorporated during the electrodeposition of Cu to increase the surface area of the electrode and modify its reactivity such that C_2H_4 production is enhanced.[22, 23] Previous studies have shown that Cu-Ag alloys are particularly adept at generating C2+ products during electrochemical CO_2 reduction. Chen *et al.* used a Cu-Ag gas diffusion electrode (GDE) that exhibited improved C_2H_4 and C_2H_5OH productivity compared to Cu alone.[24]

The electrochemical reduction of CO_2 involves a complex pathway requiring multiple electron and proton transfer steps. Due to the multiple electron and proton transfers, the selective reduction of CO_2 is difficult to achieve, especially at low overpotentials. Tandem electrocatalysis decouples individual steps with multicomponent catalyst design.[1] This method is attractive for the selective generation of C2+ products because CO_2 can first be reduced to CO on one portion of the electrode before subsequent C-C coupling yields C2+ products. The preconversion of CO_2 to CO allows for a high local concentration of CO on the surface of the electrode, which favors C-C coupling.[1]

Our group recently demonstrated that Nafion-modified metal catalysts possess unique CO_2 reduction reactivity.[25] In particular, a Nafion-modified Cu electrode exhibited a high Faradaic efficiency for CH_4 production of 88%. For this catalyst, the Nafion overlayer activates the CO bond, facilitating the further reduction of CO to CH_4. Because C2+ products require the generation of a CO intermediate, we hypothesize that Nafion-modified electrodes that enable tandem electrocatalysis could yield C2+ products. Furthermore, Nafion is a hydrophilic polymer that facilitates rapid proton transfer, which is needed for the generation of C2+ products except for oxalate. For these reasons, in this work, we use Nafion as a scaffold to host a second catalyst in combination with a metal electrode catalyst to create a tandem electrocatalyst architecture. While Nafion is commonly used as a binder in preparing electrocatalyst inks[26] or as a free-standing membrane in a divided electrolytic cell,[27] in this work, Nafion is used as an overlayer to control product selectivity and serve as a framework for tandem catalysis.

Based on previous literature showing the excellent ability of Cu-Ag alloys to generate C_2H_4,[18] we incorporated Ag and Cu catalysts into a tandem catalyst architecture. We investigated the incorporation of nanoparticle tandem catalysts inside the Nafion layer of membrane-modified electrodes. In particular, we select Ag as the metal electrode because of its high Faradaic efficiency for CO.[28] By coupling Ag electrodes with membrane-bound CO reduction catalysts, we hypothesized that the selectivity of the overall tandem catalysis process could be tuned. We began our work by studying Cu_2O nanoparticles as the membrane-bound catalysts because these nanoparticles have previously been shown to produce a variety of value-added C2 products such as C_2H_4 and ethanol with good Faradaic efficiencies.[29, 30]

Methods

Materials and Electrode Preparation

A dispersion of Nafion D520 was purchased from Fuel Cell Store. Cu foil (99.99% purity) was purchased from All-Foils, Inc. Ni and Ti foils (99.9% purity) were purchased from Goodfellow, Inc. Ag coins (99.9% purity) were purchased from APMEX and polished with sand paper until a smooth surface was obtained and rinsed with water before use. Cu_2O (18 nm in diameter, 99.86% purity), CuO (10 nm in diameter, 99% purity), Cu (40 nm in diameter, 99.% purity), and Ag (20 nm in diameter, 99.9% purity) nanoparticles were purchased from U.S. Research Nanomaterials, Inc. The larger Cu_2O nanoparticles (350 nm in diameter) were purchased from Sigma Aldrich. Sodium bicarbonate was purchased from Sigma Aldrich. CO_2 and N_2 gasses were purchased from Airgas. Electrodes were modified with Nafion layers by drop-casting a Nafion or Nafion-nanoparticle dispersion directly onto the substrate and letting the dispersion under ambient conditions. Multiple rounds of drop-casting were utilized to tune the thickness of the overlayers. Dispersions of nanoparticles in Nafion were made by sonicating 33 wt. % of the nanoparticles in the Nafion D520 for 15 minutes.

Electrochemical Measurements and Material Characterization

Electrochemical data were collected using a VSP-300 Biologic Potentiostat and were measured versus a Ag/AgCl reference electrode and converted to the reversible hydrogen electrode (RHE) scale by $V_{(vs.\ RHE)} = V_{(measured\ vs.\ Ag/AgCl)} + 0.21 + 0.059*6.8$ (where 6.8 is the pH of solution). The geometric area of the electrodes is used for current density calculations. For chronoamperometry experiments, the geometric working electrode area was 5.0 cm^2. For linear sweep voltammetry experiments, the geometric working electrode area was 0.22 cm^2. The electrolyte consisted of a 0.1 M sodium bicarbonate buffer sparged with CO_2 or N_2 gas for at least 30 min using a one-compartment, three-electrode configuration. SEM-EDX analyses using an accelerating voltage of 15 kV were obtained using a JEOL JSM-7100F field emission SEM.

Product Determination

Electrochemical reactions were performed using chronoamperometry for one hour using carbon as a counter electrode in a beaker for determining liquid and solid products and Pt wire as a counter electrode in a custom-made cell for determining gas products (Figure S1). For liquid and solid products, the geometric area of the counter electrode area was about 19 cm^2. Because this area is much larger than the geometric area of the working electrode (5.0 cm^2), the voltage applied to the counter electrode by the potentiostat during chronoamperometry was small (<100 mV). This voltage on the counter electrode is too small to oxidize any CO_2 reduction products, which is a concern for undivided cells using smaller counter electrodes. Instead, the counter electrode charge balances CO_2 reduction at the working electrode through oxidative non-Faradaic processes. This interpretation is confirmed by results using this undivided cell that yield CO_2 reduction product distributions for a wide variety of unmodified polycrystalline metals that match previous literature reports using divided cells.[25] During chronoamperometry, for all experiments, CO_2 was continuously sparged through the solution (2.5 mL) at a rate of 5 cm^3/min. For gaseous product detection, this flow rate ensures that any gaseous products are swept away from the Pt counter electrode and are out of solution before they can be oxidized.

Solid products (formate) were quantified using a Varian 400 MHz NMR Spectrometer using DMF as an internal standard. After chronoamperometry, the water in the electrolyte was evaporated under reduced pressure, and sodium formate along with other residual solids were collected and dissolved in D_2O. Liquid products were quantified using an Agilent 7890A gas chromatograph coupled to a 5975C quadrupole mass spectrometer (GC-MS). After chronoamperometry, an equal volume of acetonitrile was added to the electrolyte, and the reaction mixture was kept overnight at -15°C. The top organic layer was then removed and dried with anhydrous Na_2SO_4 before GC-MS analysis was conducted. Gas products were quantified using an SRI 8610C gas chromatograph equipped with a flame ionization detector and a methanizer. The limits of detection for formate, liquid products, and gas products were determined to be 11 μM, 5 μM, and 1 ppm, respectively. Calibration curves with products of known concentrations were used to account for any inefficiencies associated with liquid-liquid extraction or gas transfer. All experiments were at least duplicated, and all error bars presented are the standard deviation among the multiple trials.

Results and Discussion

To test the hypothesis that a tandem Ag electrode modified with a mixture of Nafion and Cu_2O nanoparticles can yield C2 products, we fabricated these electrodes and derivatives thereof by drop-casting a dispersion of 18 nm Cu_2O nanoparticles and Nafion onto Ag electrodes. By performing multiple rounds of drop-casting, the thickness of the membrane overlayer can be tuned. For example, a cross-sectional scanning electron microscopy (SEM) image of a Ag/Nafion-Cu_2O electrode constructed using five rounds of drop casting shows that the Nafion-Cu_2O layer is approximately 8 μm thick (Figure 1A). Elemental maps from energy-dispersive X-ray spectroscopy (EDX) give further information about the electrode architecture. A Ag signal is only detected from the Ag electrode substrate (Figure 1B), while F and Cu signals are only present in the Nafion-Cu_2O overlayer (Figures 1C and 1D). The F component originates from the fluorinated Nafion polymer, while the Cu comes from the nanoparticles. Taken together, these elemental maps indicate that the Ag/Nafion-Cu_2O electrode consists of a uniform composite of Nafion and Cu_2O nanoparticles on top of the Ag surface.

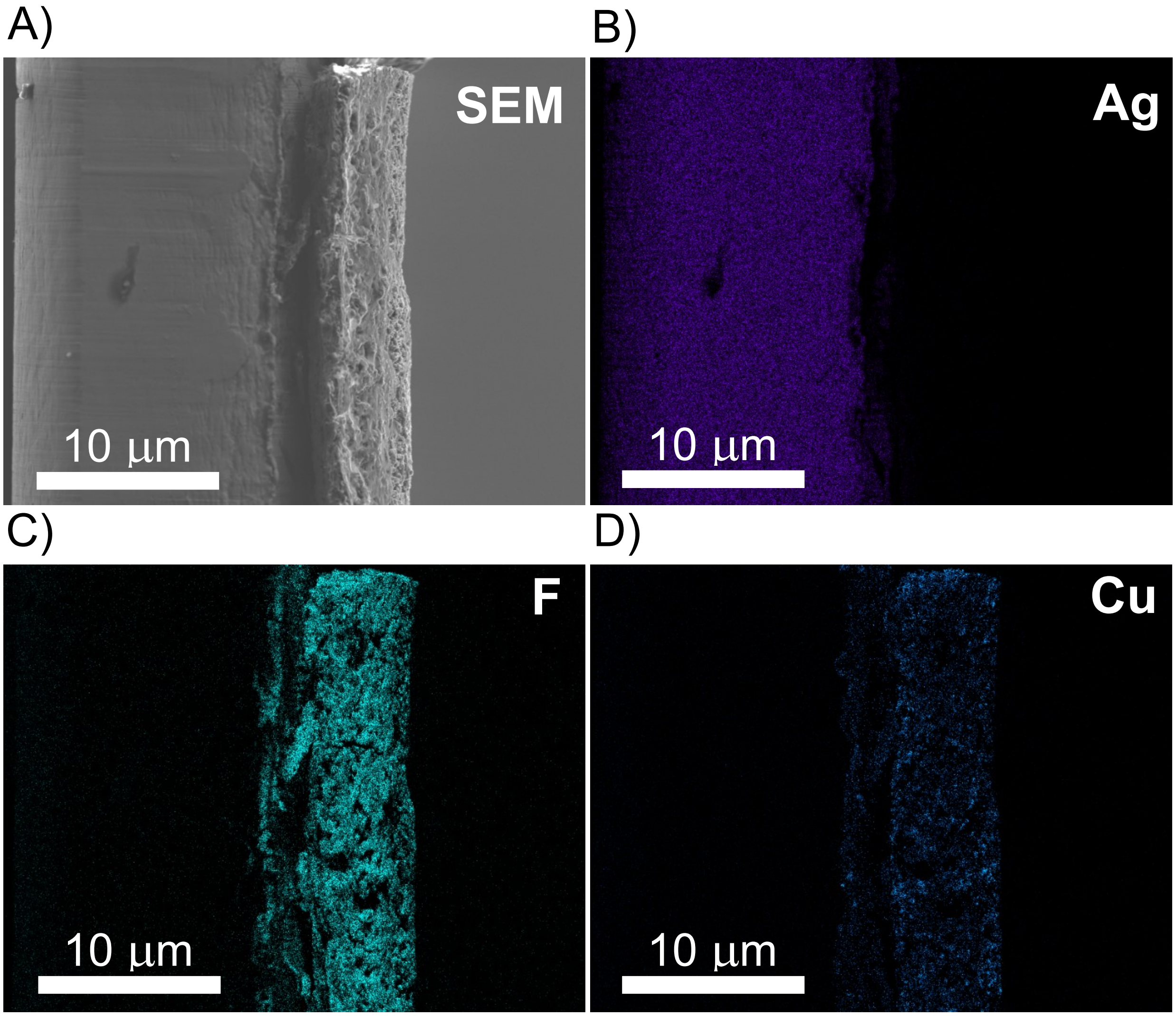

Figure 1: SEM image (A) and corresponding EDX elemental maps for Ag (B), F (C), and Cu (D) of a Ag/Nafion-Cu_2O electrode.

We next evaluated the product distribution of CO_2 reduction of these membrane-modified electrodes as elicited by chronoamperometry (Figure 2). The Faradaic efficiencies of various electrodes are presented in Figure 2A, while the rates of product formation are displayed in Figure 2B. We note that the charge densities are low compared to several previous studies of CO_2 reduction catalysts.[30] These charge densities and corresponding current densities (Figures S4-S8) are expected because the electrodes used in this study are flat, unlike porous electrodes with high surface areas.[31] Moreover, the rate of formation of CO_2 reduction products such as C_2H_4 that require more electrons per CO_2 (i.e. 12 e^-) is proportionally diminished compared to their Faradaic efficiencies or the rates of product formations that require fewer electrons per CO_2 (e.g. 2 e^- for CO or HCOOH). These patterns are consequences of the varying electron requirements to generate the different products.

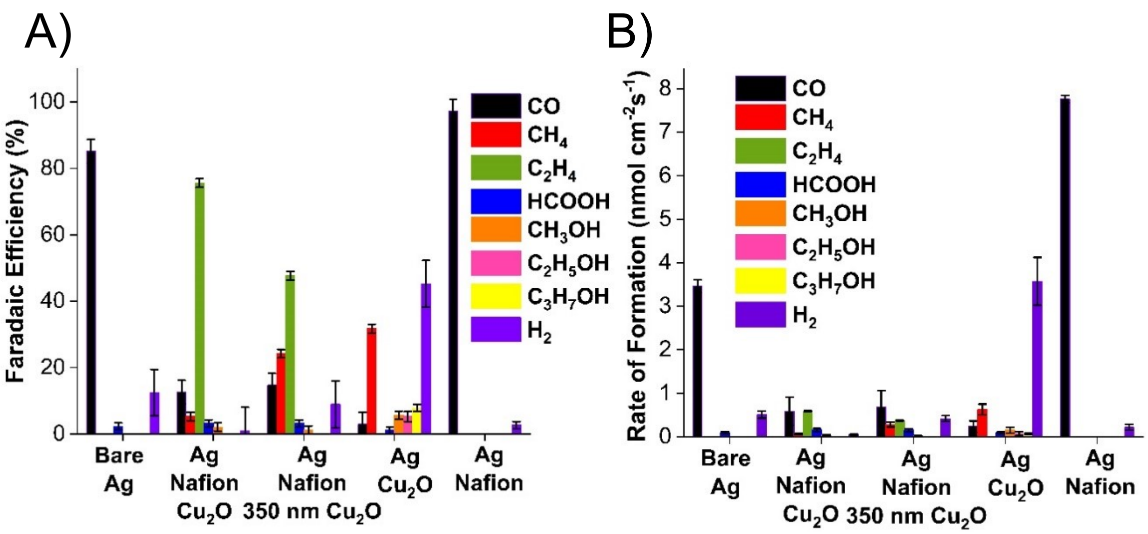

Figure 2: Faradaic efficiencies (A) and rates of formation (B) for CO (black), CH_4 (red), C_2H_4 (green), HCOOH (blue), CH_3OH (orange), C_2H_5OH (pink), C_3H_7OH (yellow), and H_2 (purple) after 1 hr of CO_2 reduction at -1.2 V vs. RHE using Ag electrodes modified with Nafion and Ag or Cu_2O nanoparticles. Both the standard-sized Cu_2O nanoparticles (18 nm in diameter) and larger Cu_2O nanoparticles (350 nm in diameter) were tested.

During 1 hour of chronoamperometry at -1.2 V vs. RHE, the Ag/Nafion-Cu_2O electrode produces ethylene (C_2H_4) as the predominant product with a Faradaic efficiency of about 76% (Figure 2A, leftmost green bar). This yield of C_2H_4 is relatively high compared to previously reported catalysts (Table S1). C1 species, CO, CH_4, HCOOH, and CH_3OH, are generated as minor products, all with Faradaic efficiencies less than 15%. More importantly, the total Faradaic efficiency for carbon-containing products is about 99%, indicating that the H_2 evolution reaction is not occurring on this electrode to any appreciable extent. We hypothesize that the high yield of C_2H_4 is due to the tandem catalysis elicited by the electrode. Specifically, CO_2 is reduced to CO on the Ag surface, and the nanoparticles within the Nafion membrane further reduce the CO to C_2H_4.

To probe the longer-term durability of the Ag/Nafion-Cu_2O electrode, we performed a six-hour CO_2 reduction experiment and measured the Faradaic efficiency for gaseous products each hour (Figure S2). Over the course of six hours, the C_2H_4 Faradaic efficiency decreased only slightly from an initial value of 78% to a final value of 74%. SEM-EDX analysis (Figure S3) demonstrates that in select areas of the Nafion film, cracks form and dendrites containing Cu grow at the interfaces of these cracks. These changes in morphology of the electrode are likely responsible for the slightly diminished C_2H_4 Faradaic efficiency after six hours of CO_2 reduction.

To evaluate the validity of this tandem reaction pathway, we determined the product distribution for CO_2 reduction on a variety of derivatives of the Ag/Nafion-Cu_2O architecture. First, we tested a Ag electrode modified with a mixture of Nafion and larger 350 nm Cu_2O nanoparticles. Like the electrode containing the 18 nm Cu_2O nanoparticles, this electrode still generates C_2H_4 as the major product. However, the Faradaic efficiency for C_2H_4 production decreases to about 48%, and the CH_4 yield increases as compared to the electrode with the smaller Cu_2O nanoparticles. Because the size of the Cu_2O nanoparticles significantly impacts the product distribution of CO_2 reduction, these two experiments demonstrate that Cu_2O nanoparticles play an active role in the CO_2 reduction process. Furthermore, when operating under the hypothesis that the Cu_2O nanoparticles facilitate C-C coupling, the higher C_2H_4 yield with the smaller Cu_2O nanoparticles is expected due to the higher surface area of these particles.

Four control experiments further support the notion of tandem catalysis in the Ag/Nafion-Cu_2O electrode. First, an unmodified Ag electrode generates CO with high selectivity, an observation that matches previous literature results.[28, 32] Second, a Ag electrode modified with

Cu_2O nanoparticles without a Nafion membrane does not yield any C_2H_4. We note that while Ag-Cu alloy catalysts produce C_2H_4,[24] the Cu_2O nanoparticles on Ag studied here did not produce C_2H_4. This experiment demonstrates that the Nafion membrane is required to generate C_2H_4 and that the membrane serves a critical function in the tandem reduction process. This lack of C_2H_4 produced in this experiment suggests that the Ag surface and the Cu_2O nanoparticles are not simply acting synergistic cocatalysts to yield C_2H_4, but rather that a tandem mechanism supported by the presence of the membrane is operative. Interestingly, the Ag/Cu_2O electrode without the membrane is the only system to generate C_2H_5OH and C_3H_7OH, albeit in small yields (<10% Faradaic efficiencies). The generation of C2+ alcohols is consistent with previous studies using Cu oxide derived electrodes.[33, 34] Third, a Ag electrode modified with a Nafion membrane and Ag nanoparticles does not result in any C_2H_4. As with the experiments with differing Cu_2O nanoparticle sizes, this experiment also indicates that Cu_2O nanoparticles in the membrane are necessary to produce C_2H_4. Fourth, a Cu electrode modified with a Nafion membrane and Ag nanoparticles yields 17% CO, 13% HCOOH, 3% CH_3OH, and 67% H_2. Interestingly, this Cu/Nafion-Ag electrode does not produce any C_2H_4. This experiment indicates that to achieve high yields of C_2H_4 in a Nafion tandem architecture, a metal electrode that produces CO selectively (i.e. Ag) should be utilized such that the CO produced can then be subsequently converted to C_2H_4 by the Nafion-bound catalyst (i.e. Cu_2O). Unlike Ag, unmodified polycrystalline Cu produces negligible amounts of CO at -1.2 V vs. RHE,[8] which explains why no C_2H_4 is produced by the Cu/Nafion-Ag system. Taken together, these experiments provide strong evidence for a tandem catalysis reaction pathway in which the Ag electrode generates CO with high selectivity, and the membrane-bound Cu_2O nanoparticles subsequently convert this CO to C_2H_4.

C_2H_4 is the typical product C2 product generated on Cu-based catalysts, but C_2H_5OH can also be produced.[35] A metal-bound M-OC_2H_3 species has been identified as the key intermediate that determines the selectivity among these two C2 products. If protonation occurs on the α carbon adjacent to the O atom, C_2H_4 is produced. On the other hand, if protonation occurs on the β carbon, C_2H_5OH is the predominant product. Under most circumstances, as is the case in this work, α carbon protonation yielding C_2H_4 is the kinetically more facile pathway.

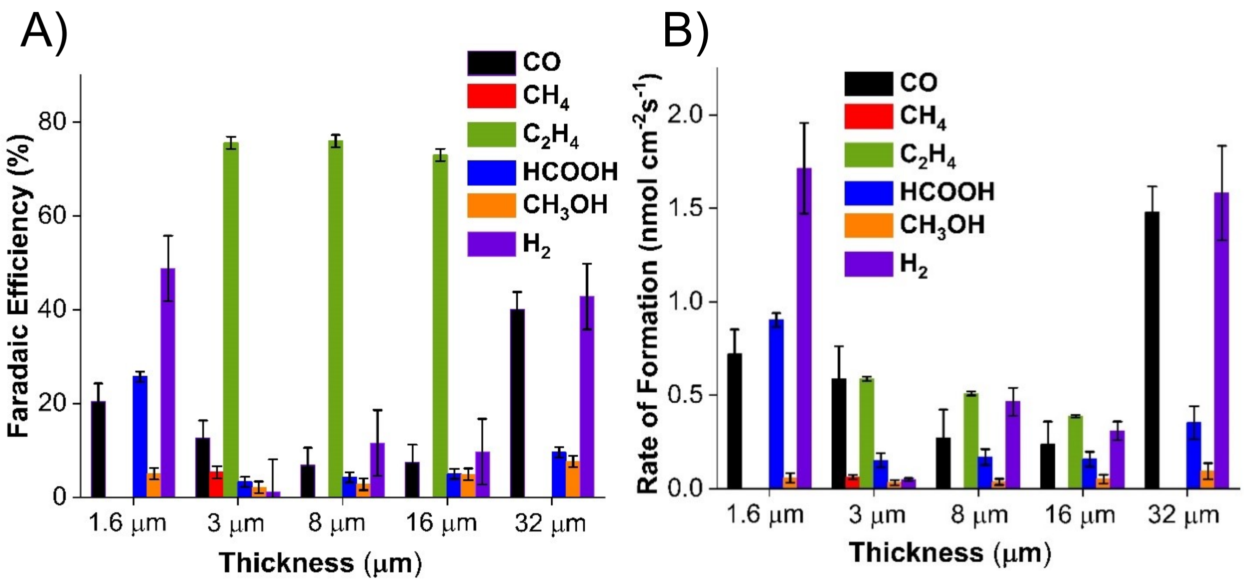

Figure 3: Faradaic efficiencies (A) and rates of formation (B) for CO (black), CH_4 (red), C_2H_4 (green), HCOOH (blue), CH_3OH (orange), and H_2 (purple) after 1 hr of CO_2 reduction at -1.2 V vs. RHE using Ag electrodes modified with a mixture of various thicknesses of Nafion and 18 nm Cu_2O nanoparticles.

We next assessed the effect of the thickness of the Nafion/Cu_2O overlayer on the CO_2 reduction product distribution (Figure 3). The results show that with membrane thicknesses between 3 μm to 16 μm, the electrodes all display similar product distributions and C_2H_4 Faradaic efficiencies greater than 70%. However, when the overlayer is too thin (i.e. 1.6 μm), no C_2H_4 is generated. We hypothesize that in this case, CO is generated at the Ag electrode, and the thin membrane does not allow enough time for the Cu_2O nanoparticles to further reduce the CO to

C_2H_4. On the other extreme, an electrode with an overlayer that is too thick (i.e. 32 μm) also does not produce any C_2H_4. The lack of C_2H_4 is likely due to impeded mass transport of CO_2 to the Ag electrode. Previous studies with Nafion-modified CO_2 reduction electrodes have shown that mass transport of CO_2 to the electrode becomes problematic with membranes of these thicknesses.[25] In this case, CO_2 reduction predominantly occurs within the Nafion-electrolyte interface instead of at the electrode-Nafion interface. As a whole, these experiments with varying overlayer thicknesses demonstrate that an optimal thickness of the Nafion/Cu_2O layer is needed to elicit tandem catalysis with the mass transport characteristics required for C_2H_4 production.

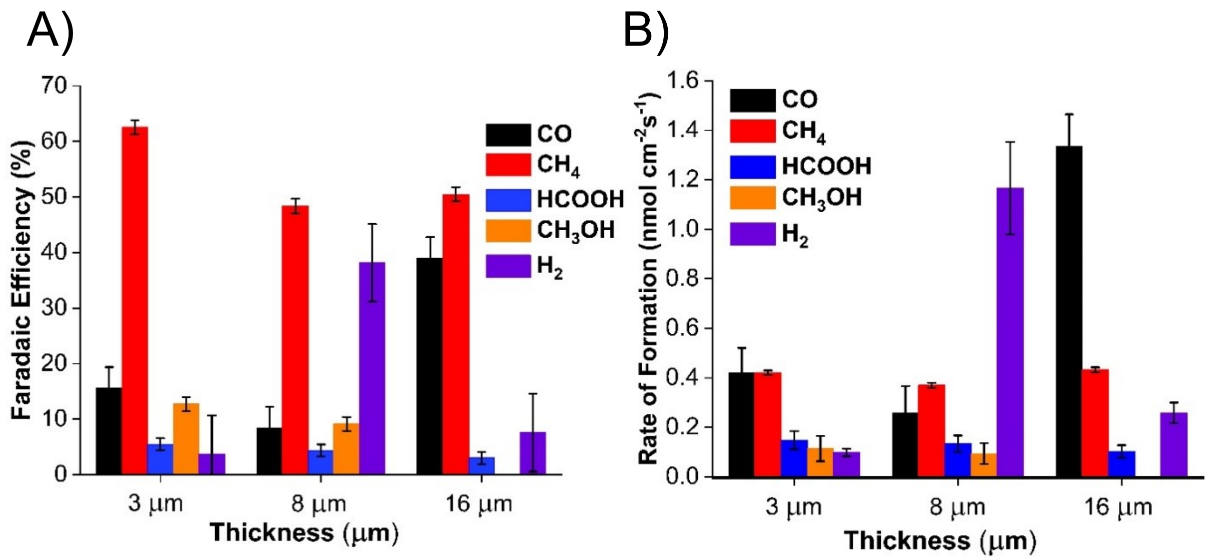

Figure 4: Faradaic efficiencies (A) and rates of formation (B) for CO (black), CH_4 (red), HCOOH (blue), CH_3OH (orange), and H_2 (purple) after 1 hr of CO_2 reduction at -0.9 V vs. RHE using Ag electrodes modified with a mixture of various thicknesses of Nafion and 18 nm Cu_2O nanoparticles.

Having established that Nafion/Cu_2O layers with thicknesses between 3 μm to 16 μm are optimal for C_2H_4 production, we next studied the effect of electrode potential on product distribution. The potential applied during CO_2 reduction is known to dramatically affect catalyst selectivity for a wide variety of systems.[36, 37] First, we performed chronoamperometry at -0.9 V vs. RHE at the optimal overlayer thicknesses (3 μm, 8 μm, and 16 μm, Figure 4). In a manner similar to the experiments conducted at -1.2 V (Figure 3), the Faradaic efficiencies for the products at these three different thicknesses did not vary significantly. However, when CO_2 reduction was elicited at -0.9 V, no C_2H_4 was detected. This finding that C_2H_4 production decreases at potentials more positive than -1.2 V is consistent with previous experiments with other Cu-based catalysts.[20, 38, 39] Although the thermodynamic potential for CO_2 reduction to C_2H_4 is within the same range as the various C1 products,[40] the overpotential for C_2H_4 production is higher due to a rate-limiting C-C coupling step.[15, 21, 41] A complete study of the effect of voltage on product distribution for the electrode with a 3 μm Nafion/Cu_2O overlayer is presented in Figure 5. Again, the data show that at voltages more positive than -1.2 V, C_2H_4 is not produced, while at higher overpotentials, the catalyst is quite selective for C_2H_4 generation with a maximum Faradaic efficiency for C_2H_4 of about 80% at -1.9 V.

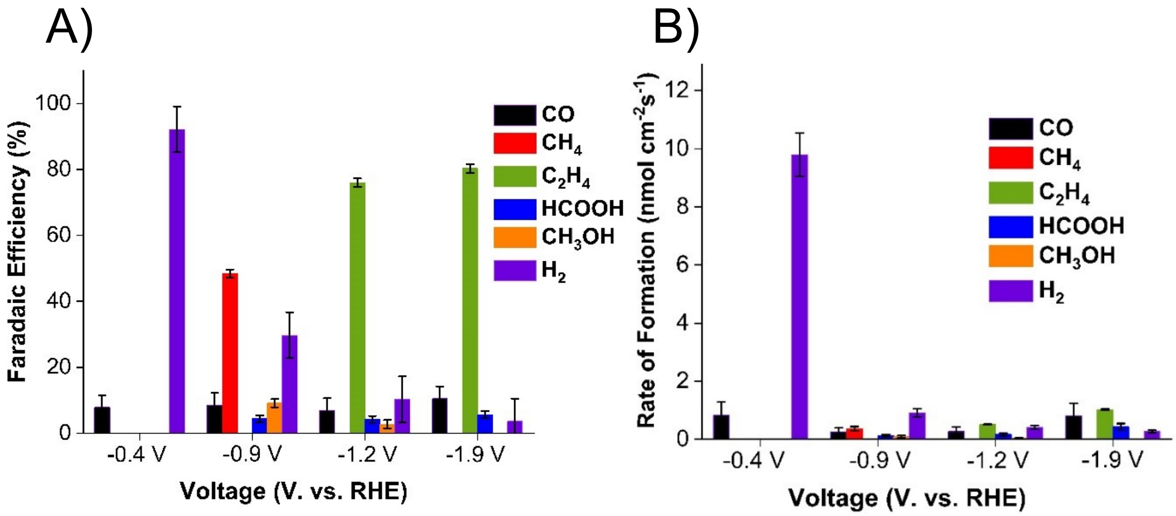

Figure 5: Faradaic efficiencies (A) and rates of formation (B) for CO (black), CH_4 (red), C_2H_4 (green), HCOOH (blue), CH_3OH (orange), and H_2 (purple) after 1 hr of CO_2 reduction at different voltages using Ag electrodes modified with a 3 μm-thick mixture of Nafion and 18 nm in diameter Cu_2O nanoparticles.

To elucidate the origin of the high C_2H_4 selectivity of the Ag/Nafion-Cu_2O architecture, we systematically varied the chemical identity of both the membrane-bound nanoparticle catalysts and the electrode catalyst. We first compared the electrochemical performance of Ag electrodes modified with mixtures of Nafion and various Cu-based nanoparticles (Figure 6). In particular, we analyzed electrodes containing membrane-bound Cu nanoparticles of similar diameter, but with different oxidation states (i.e. Cu, Cu_2O, and CuO). Regardless of the oxidation state of Cu in the nanoparticles, the Faradaic efficiency for C_2H_4 production is greater than 70%, and in general, the three product distributions among the three different nanoparticles are very similar. This finding suggests that the active catalytic species in all three nanoparticles is the same. We hypothesize that when the nanoparticles are subjected to the negative potential used (e.g. -1.2 V) during CO_2 reduction, the Cu in the Cu_2O or CuO nanoparticles is electrochemically reduced to Cu (0).

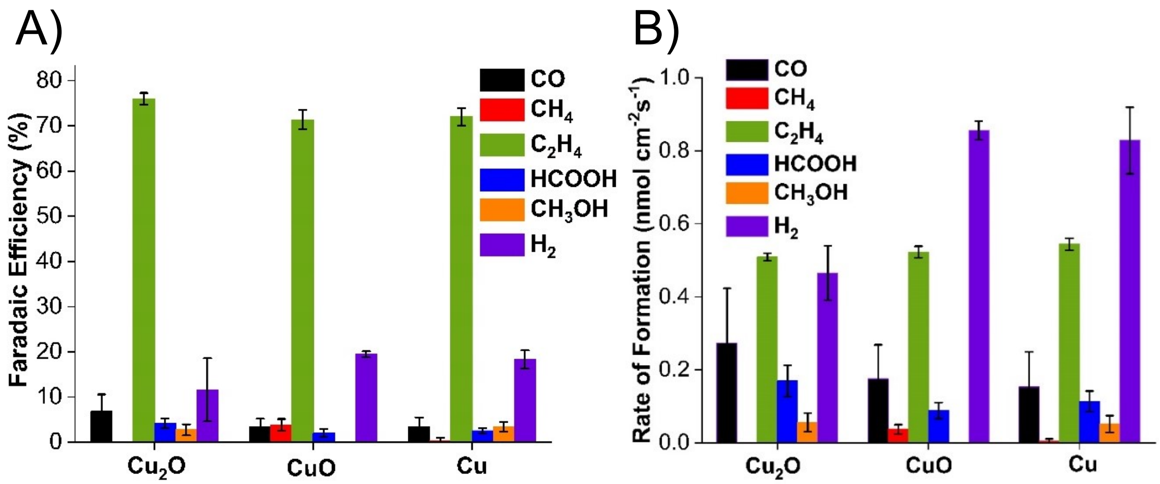

Figure 6: Faradaic efficiencies (A) and rates of formation (B) for CO (black), CH_4 (red), C_2H_4 (green), HCOOH (blue), CH_3OH (orange), and H_2 (purple) after 1 hr of CO_2 reduction at -1.2 V vs. RHE using Ag electrodes modified with a 8 µm-thick mixture of various thicknesses of Nafion and Cu_2O, CuO, or Cu nanoparticles.

To test this hypothesis, we performed linear sweep voltammetry (LSV) of the various Ag/Nafion-CuO_x electrodes during CO_2 reduction (Figure 7). A LSV of a Ag electrode modified with Nafion without nanoparticles displays one reductive peak at around 0.1 V (Figure 7, blue line and blue arrow), which is due to the reduction of electrochemically generated Ag(I) to Ag(0). Similarly, a LSV of a Ag electrode modified with Nafion with Cu nanoparticles exhibits one reduction peak due to the same process (Figure 7, green line and green arrow). However, a LSV of a Ag electrode with a Nafion/Cu_2O overlayer contains two reductive peaks (Figure 7, black line and black arrows). The Ag(I)/Ag(0) peak at about 0.1 V is present, but there is also a second peak at around -0.4 V, which is presumably due to the reduction of the Cu(I) in the nanoparticles to Cu(0). Following this trend, a LSV of a Ag electrode with a Nafion/CuO overlayer displays three reductive peaks (Figure 7, red line and red arrows), one due to Ag(I)/Ag(0) and two additional peaks due to the Cu(II)/Cu(I) and Cu(I)/Cu(0) redox processes. Because the chronoamperometry used to elicit CO_2 reduction is performed at a voltage significantly more negative (e.g. -1.2 V) than all of these reductive peaks, we conclude that the active species in the nanoparticles during CO_2 reduction for any of the three Ag/Nafion-CuO_x systems is Cu(0). These results explain why the product distributions of the three Ag/Nafion-CuO_x electrodes are similar regardless of the oxidation state of the CuO_x nanoparticles in the membrane overlayer (Figure 6).

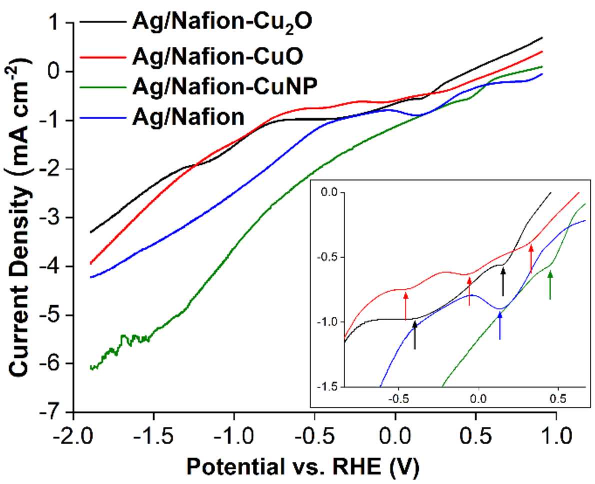

Figure 7: Linear sweep voltammograms of Ag electrodes modified with a 8 μm-thick Nafion layer (blue) mixed with nanoparticles of Cu_2O (black), CuO (red), or Cu (green) in CO_2-sparged 100 mM $NaHCO_3$ at a scan rate of 10 mV/s. Inset (boxed plot) shows the voltammograms from +0.7 V to -0.8 V vs. RHE, and the arrows label reduction peaks.

In addition to modulating the chemical composition of the membrane-bound nanoparticles, we also altered the chemical composition of the electrodes and analyzed their CO_2 reduction production distributions (Figure 8). Ti/Nafion-Cu_2O and Ni/Nafion-Cu_2O electrodes produce relatively low Faradaic efficiencies of carbon-containing products. It is known that unmodified Ti and Ni both produce large amounts of H_2 during CO_2 electroreduction.[28, 42] It is unsurprising then that these metals generate low Faradaic efficiencies of carbon-containing products in the membrane-modified tandem architecture as well. A Cu/Nafion-Cu_2O electrode similarly yields low Faradaic efficiencies of carbon-containing products. Depending upon the exact conditions used, unmodified Cu electrodes produce a wide variety of carbon-containing products, albeit usually with poor selectivity for any one product.[28, 43] Importantly though, unmodified polycrystalline Cu electrodes generate low yields of CO.[8] For this reason, we speculate that for the Cu/Nafion-Cu_2O electrode, there is not enough CO to be further reduced to C_2H_4 on the surface of the Cu_2O nanoparticles.

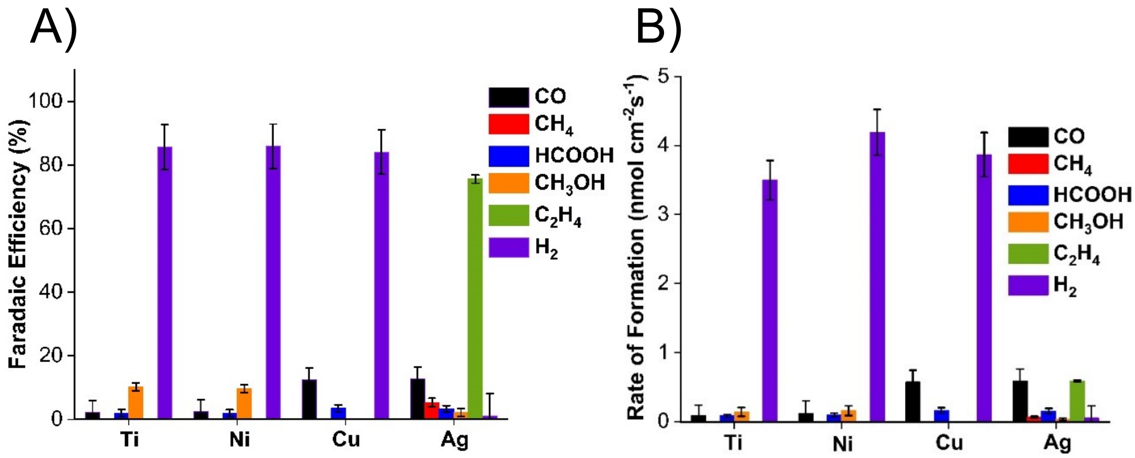

Figure 8: Faradaic efficiencies (A) and rates of formation (B) for CO (black), CH_4 (red), C_2H_4 (green), HCOOH (blue), CH_3OH (orange), and H_2 (purple) after 1 hr of CO_2 reduction at -1.2 V vs. RHE using different metal electrodes modified with a 3 μm-thick layer of Nafion and 18 nm Cu_2O nanoparticles.

Taken together, these results indicate that the combination of a Ag electrode with the membrane-bound CuO_x nanoparticles gives rise to unique synergism that results in selective C_2H_4 production. The origin of the high Faradaic efficiency of C_2H_4 from Ag/Nafion-CuO_x electrodes comes from both the Ag electrode's ability to generate CO at the polymer-electrode interface with good selectivity and for C-C coupling to be catalyzed by the membrane-bound Cu nanoparticles. In other words, these results demonstrate that the Ag/Nafion-CuO_x electrode produces C_2H_4 via a tandem pathway (Figure 9).

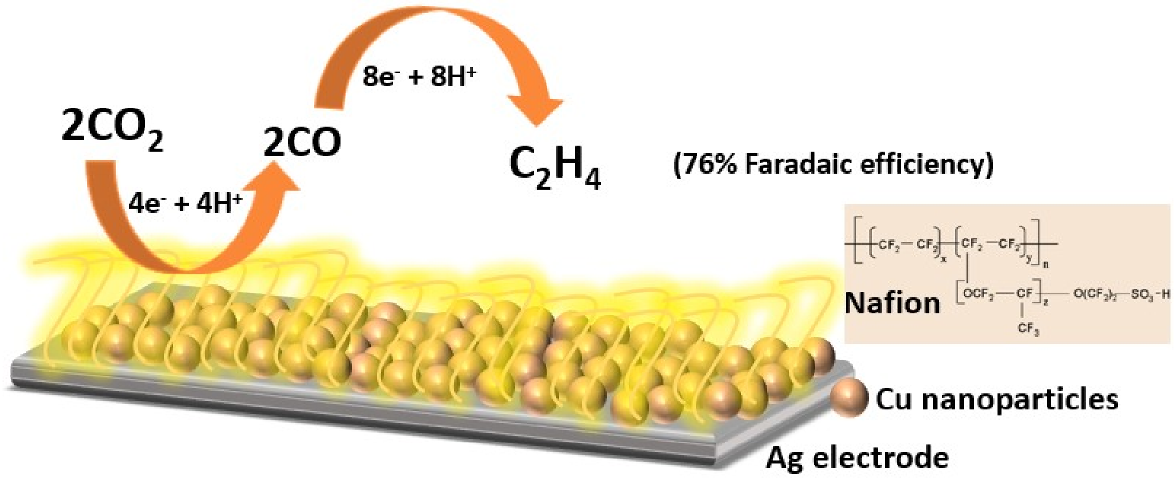

Figure 9: Schematic of tandem reduction of CO_2 to C_2H_4 on a Ag electrode modified with a mixture of Nafion and Cu nanoparticles.

Conclusions

In this manuscript, we design novel tandem catalysts based on Ag electrodes modified with membrane-bound CuO_x nanoparticles for selective electrocatalytic reduction of CO_2 to C_2H_4. By systematically changing the physical and chemical attributes of the electrode architecture, we determine that these catalysts operate via a stepwise pathway in which CO_2 is first reduced to CO on the Ag surface, and the formed CO is subsequently reduced to C_2H_4 on the surface of the CuO_x nanoparticles. Faradaic efficiencies for C_2H_4 as high as 80% are obtained, and this high Faradaic efficiency is only achievable with a Ag electrode and an optimal thickness of the Nafion/CuO_x overlayer. An analogous Ag-Cu catalyst without the Nafion overlayer does not produce any C_2H_4, which testifies to the role the polymer layer plays in controlling the mass transport of the reactive CO intermediate. Not only is the design of CO_2 reduction catalysts with high C_2H_4 selectivity industrially relevant, the developed membrane-enabled tandem pathway could also be applied to future CO_2 catalytic systems to enable the selective production of other value-added C2+ products.

Supporting Information.

Chronoamperometry data, SEM-EDX data, and a schematic of the cell used for gaseous product detection.

AUTHOR INFORMATION
Corresponding Author
*E-mail: cbarile@unr.edu

ORCID

Christopher J. Barile: 0000-0002-4893-9506

Notes

The authors declare no completing financial interest.

Acknowledgments

This material is based upon work supported by the National Science Foundation CAREER Award under Grant No. CHE-2046105. This research was supported by Research and Innovation at the University of Nevada, Reno (UNR). SEM-EDS analysis was done in the Mackay Microbeam Laboratory at UNR, we acknowledge J. DesOrmeau for his kind assistance. We acknowledge the Shared Instrumentation Laboratory in the Department of Chemistry at UNR.

References

1. Morales-Guio, C. G.; Cave, E. R.; Nitopi, S. A.; Feaster, J. T.; Wang, L.; Kuhl, K. P.; Jackson, A.; Johnson, N. C.; Abram, D. N.; Hatsukade, T.; Hahn, C.; Jaramillo, T. F. Improved CO_2 Reduction Activity Towards C2+ Alcohols on a Tandem Gold on Copper Electrocatalyst. *Nat. Catal.* **2018**, *1*, 764-771.

2. Popović, S.; Smiljanić, M.; Jovanovič, P.; Vavra, J.; Buonsanti, R.; Hodnik, N. Stability and Degradation Mechanisms of Copper-Based Catalysts for Electrochemical CO_2 Reduction. *Angew. Chem.* **2020,** *59*, 14736-14746.

3. Whipple, D. T.; Kenis, P. J. A. Prospects of CO_2 Utilization via Direct Heterogeneous Electrochemical Reduction. *J. Phys. Chem. Lett.* **2010**, *1*, 3451-3458.

4. Arakawa, H.; Aresta, M.; Armor, J. N.; Barteau, M. A.; Beckman, E. J.; Bell, A. T.; Bercaw, J. E.; Creutz, C.; Dinjus, E.; Dixon, D. A. et al. Catalysis Research of Relevance to Carbon Management: Progress, Challenges, and Opportunities. *Chem. Rev.* **2001**, *101*, 953-996.

5. Qiao, J.; Liu, Y.; Hong, F.; Zhang, J. A Review of Catalysts for the Electroreduction of Carbon Dioxide to Produce Low-carbon Fuels. *Chem. Soc. Rev.* **2014**, *43*, 631-675.

6. Hori, Y., Electrochemical CO_2 Reduction on Metal Electrodes. In *Modern Aspects of Electrochemistry*, Vayenas, C. G.; White, R. E.; Gamboa-Aldeco, M. E., Eds. Springer New York: New York, NY, 2008; pp 89-189.

7. Kuhl, K. P.; Hatsukade, T.; Cave, E. R.; Abram, D. N.; Kibsgaard, J.; Jaramillo, T. F., Electrocatalytic Conversion of Carbon Dioxide to Methane and Methanol on Transition Metal Surfaces. *J. Am. Chem. Soc.* **2014**, *136*, 14107-14113.

8. Kuhl, K. P.; Cave, E. R.; Abram, D. N.; Jaramillo, T. F. New Insights into the Electrochemical Reduction of Carbon Dioxide on Metallic Copper Surfaces. *Energy. Environ. Sci.* **2012**, *5*, 7050-7059.

9. Hatsukade, T.; Kuhl, K. P.; Cave, E. R.; Abram, D. N.; Jaramillo, T. F. Insights into the Electrocatalytic Reduction of CO_2 on Metallic Silver Surfaces. *Phys. Chem. Chem. Phys.* **2014**, *16*, 13814-13819.

10. Torelli, D. A.; Francis, S. A.; Crompton, J. C.; Javier, A.; Thompson, J. R.; Brunschwig, B. S.; Soriaga, M. P.; Lewis, N. S. Nickel-Gallium-Catalyzed Electrochemical Reduction of CO_2 to Highly Reduced Products at Low Overpotentials. *ACS Catal.* **2016**, *6*, 2100-2104.

11. Hori, Y.; Murata, A. Electrochemical Evidence of Intermediate Formation of Adsorbed CO in Cathodic Reduction of CO_2 at a Nickel Electrode. *Electrochim. Acta* **1990**, *35*, 1777-1780.

12. Gao, S.; Lin, Y.; Jiao, X.; Sun, Y.; Luo, Q.; Zhang, W.; Li, D.; Yang, J.; Xie, Y. Partially Oxidized Atomic Cobalt Layers for Carbon Dioxide Electroreduction to Liquid Fuel. *Nature* **2016**, *529*, 68-71.

13. Birdja, Y. Y.; Pérez-Gallent, E.; Figueiredo, M. C.; Göttle, A. J.; Calle-Vallejo, F.; Koper, M. T. M. Advances and Challenges in Understanding the Electrocatalytic Conversion of Carbon Dioxide to Fuels. *Nat. Energy* **2019**, *4*, 732-745.

14. Jiang, Y.; Choi, C.; Hong, S.; Chu, S.; Wu, T. S.; Soo, Y. L.; Hao, L.; Jung, Y.; Sun, Z., Enhanced Electrochemical CO_2 Reduction to Ethylene over CuO by Synergistically Tuning Oxygen Vacancies and Metal Doping. *Cell. Rep. Phys. Sci.* **2021**, *2*, 100356-100370.

15. Mangione, G.; Huang, J.; Buonsanti, R.; Corminboeuf, C., Dual-Facet Mechanism in Copper Nanocubes for Electrochemical CO_2 Reduction into Ethylene. *J. Phys. Chem. Lett.* **2019**, *10*, 4259-4265.

16. De Gregorio, G. L.; Burdyny, T.; Loiudice, A.; Iyengar, P.; Smith, W. A.; Buonsanti, R., Facet-Dependent Selectivity of Cu Catalysts in Electrochemical CO_2 Reduction at Commercially Viable Current Densities. *ACS Catal.* **2020**, *10*, 4854-4862.

17. Loiudice, A.; Lobaccaro, P.; Kamali, E. A.; Thao, T.; Huang, B. H.; Ager, J. W.; Buonsanti, R., Tailoring Copper Nanocrystals towards C2 Products in Electrochemical CO_2 Reduction. *Angew. Chem.* **2016**, *55*, 5789-5792.

18. Chen, Y.; Fan, Z.; Wang, J.; Ling, C.; Niu, W.; Huang, Z.; Liu, G.; Chen, B.; Lai, Z.; Liu, X. et al. Ethylene Selectivity in Electrocatalytic CO_2 Reduction on Cu Nanomaterials: A Crystal Phase-Dependent Study. *J. Am. Chem. Soc.* **2020**, *142*, 12760-12766.

19. Jeon, H. S.; Kunze, S.; Scholten, F.; Roldan Cuenya, B. Prism-Shaped Cu Nanocatalysts for Electrochemical CO_2 Reduction to Ethylene. *ACS Catal.* **2018**, *8*, 531-535.

20. Lee, S. Y.; Jung, H.; Kim, N. K.; Oh, H. S.; Min, B. K.; Hwang, Y. J. Mixed Copper States in Anodized Cu Electrocatalyst for Stable and Selective Ethylene Production from CO_2 Reduction. *J. Am. Chem. Soc.* **2018**, *140*, 8681-8689.

21. Chou, T. C.; Chang, C. C.; Yu, H. L.; Yu, W. Y.; Dong, C. L.; Velasco-Vélez, J. J.; Chuang, C. H.; Chen, L. C.; Lee, J. F.; Chen, J. M. et al. Controlling the Oxidation State of the Cu Electrode and Reaction Intermediates for Electrochemical CO_2 Reduction to Ethylene. *J. Am. Chem. Soc.* **2020**, *142*, 2857-2867.

22. Chen, X.; Chen, J.; Alghoraibi, N. M.; Henckel, D. A.; Zhang, R.; Nwabara, U. O.; Madsen, K. E.; Kenis, P. J. A.; Zimmerman, S. C.; Gewirth, A. A. Electrochemical CO_2-to-ethylene Conversion on Polyamine-incorporated Cu Electrodes. *Nat. Catal.* **2021**, *4*, 20-27.

23. Hoang, T. T. H.; Ma, S.; Gold, J. I.; Kenis, P. J. A.; Gewirth, A. A. Nanoporous Copper Films by Additive-Controlled Electrodeposition: CO_2 Reduction Catalysis. *ACS Catal.* **2017**, *7*, 3313-3321.

24. Chen, X.; Henckel, D. A.; Nwabara, U. O.; Li, Y.; Frenkel, A. I.; Fister, T. T.; Kenis, P. J. A.; Gewirth, A. A. Controlling Speciation during CO_2 Reduction on Cu-Alloy Electrodes. *ACS Catal.* **2020**, *10*, 672-682.

25. Pan, H.; Barile, C. J. Electrochemical CO_2 Reduction to Methane with Remarkably High Faradaic Efficiency in the Presence of a Proton Permeable Membrane. *Energy. Environ. Sci.* **2020**, *13*, 3567-3578.

26. Prakash, G. K. S.; Viva, F. A.; Olah, G. A. Electrochemical Reduction of CO_2 over Sn-Nafion Coated Electrode for a Fuel-Cell-Like Device. *J. Power Sources* **2013**, *223*, 68-73.

27. Dewulf, D. W.; Bard, A. J. The Electrochemical Reduction of CO_2 to CH_4 and C_2H_4 at Cu/Nafion Electrodes (Solid Polymer Electrolyte Structures). *Catal. Lett.* **1988**, *1*, 73-79.

28. Hori, Y.; Wakebe, H.; Tsukamoto, T.; Koga, O., Electrocatalytic Process of CO Selectivity in Electrochemical Reduction of CO_2 at Metal Electrodes in Aqueous Media. *Electrochim. Acta* **1994**, *39*, 1833-1839.

29. Song, Y.; Peng, R.; Hensley, D. K.; Bonnesen, P. V.; Liang, L.; Wu, Z.; Meyer Iii, H. M.; Chi, M.; Ma, C.; Sumpter, B. G. et al. High-Selectivity Electrochemical Conversion of CO_2 to Ethanol using a Copper Nanoparticle/N-Doped Graphene Electrode. *ChemistrySelect* **2016**, *1*, 6055-6061.

30. Kim, J.; Choi, W.; Park, J. W.; Kim, C.; Kim, M.; Song, H. Branched Copper Oxide Nanoparticles Induce Highly Selective Ethylene Production by Electrochemical Carbon Dioxide Reduction. *J. Am. Chem. Soc.* **2019**, *141*, 6986-6994.

31. Grdeń, M. Impedance Study on the Capacitance of Silver Electrode Oxidised in Alkaline Electrolyte. *J. Solid State Electrochem.* **2017**, *21*, 3333-3344.

32. Qi, K.; Zhang, Y.; Li, J.; Charmette, C.; Ramonda, M.; Cui, X.; Wang, Y.; Zhang, Y.; Wu, H.; Wang, W.; Zhang, X. et al. Enhancing the CO_2-to-CO Conversion from 2D Silver Nanoprisms via Superstructure Assembly. *ACS Nano* **2021**, *15*, 7682-7693.

33. Lei, Q.; Zhu, H.; Song, K.; Wei, N.; Liu, L.; Zhang, D.; Yin, J.; Dong, X.; Yao, K.; Wang, N. et al. Investigating the Origin of Enhanced C2+ Selectivity in Oxide-/Hydroxide-Derived Copper Electrodes during CO_2 Electroreduction. *J. Am. Chem. Soc.* **2020**, *142*, 4213-4222.

34. Gu, Z.; Shen, H.; Chen, Z.; Yang, Y.; Yang, C.; Ji, Y.; Wang, Y.; Zhu, C.; Liu, J.; Li, J. et al. Efficient Electrocatalytic CO_2 Reduction to C2+ Alcohols at Defect-Site-Rich Cu Surface. *Joule* **2021**, *5*, 429-440.

35. Yang, K. D.; Lee, C.; Jin, K.; Im, S.; Nam, K. Current Status and Bioinspired Perspective of Electrochemical Conversion of CO_2 to a Long-Chain Hydrocarbon. *J. Phys. Chem. Lett.* **2017**, *8*, 538-545.

36. Ren, D.; Fong, J.; Yeo, B. S. The Effects of Currents and Potentials on the Selectivities of Copper toward Carbon Dioxide Electroreduction. *Nat. Commun.* **2018**, *9*, 925-932.

37. Sun, Z.; Ma, T.; Tao, H.; Fan, Q.; Han, B. Fundamentals and Challenges of Electrochemical CO_2 Reduction Using Two-Dimensional Materials. *Chem* **2017**, *3*, 560-587.

38. Ma, W.; Xie, S.; Liu, T.; Fan, Q.; Ye, J.; Sun, F.; Jiang, Z.; Zhang, Q.; Cheng, J.; Wang, Y. Electrocatalytic Reduction of CO_2 to Ethylene and Ethanol through Hydrogen-assisted C–C Coupling over Fluorine-modified Copper. *Nat. Catal.* **2020**, *3*, 478-487.

39. Zhang, W.; Huang, C.; Xiao, Q.; Yu, L.; Shuai, L.; An, P.; Zhang, J.; Qiu, M.; Ren, Z.; Yu, Y., Atypical Oxygen-Bearing Copper Boosts Ethylene Selectivity toward Electrocatalytic CO_2 Reduction. *J. Am. Chem. Soc.* **2020**, *142*, 11417-11427.

40. Barlow, J. M.; Yang, J. Y., Thermodynamic Considerations for Optimizing Selective CO_2 Reduction by Molecular Catalysts. *ACS Cent. Sci.* **2019**, *5*, 580-588.

41. Todorova, T. K.; Schreiber, M. W.; Fontecave, M., Mechanistic Understanding of CO2 Reduction Reaction (CO_2RR) Toward Multicarbon Products by Heterogeneous Copper-Based Catalysts. *ACS Catalysis* **2020**, *10*, 1754-1768.

42. Liu, C.; Cundari, T. R.; Wilson, A. K. CO_2 Reduction on Transition Metal (Fe, Co, Ni, and Cu) Surfaces: In Comparison with Homogeneous Catalysis. *J. Phys. Chem. C.* **2012**, *116*, 5681-5688.

43. Nitopi, S.; Bertheussen, E.; Scott, S. B.; Liu, X.; Engstfeld, A. K.; Horch, S.; Seger, B.; Stephens, I. E. L.; Chan, K.; Hahn, C. et al. Progress and Perspectives of Electrochemical CO_2 Reduction on Copper in Aqueous Electrolyte. *Chem. Rev.* **2019**, *119*, 7610-7672.

TOC Graphic

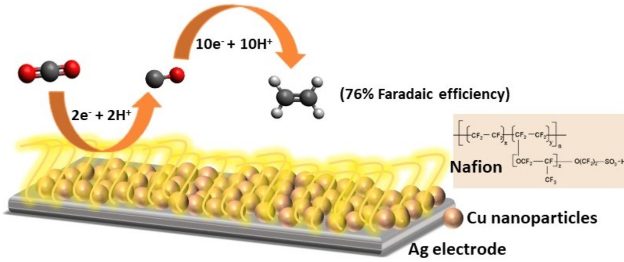
10e⁻ + 10H⁺
2e⁻ + 2H⁺
(76% Faradaic efficiency)
Nafion
Cu nanoparticles
Ag electrode